horticulturae

MDPI

Article

MIR396d-p3 Negatively Regulates Apple Resistance to *Colletotrichum gloeosporioides* via *MdUGT89A2* and *MdRGA3*

Baodong Zhang [1], Jinqi Tang [2], Zhirui Ji [1], Yinan Du [1], Jialin Cong [1] and Zongshan Zhou [1,*]

[1] Research Institute of Pomology, Chinese Academy of Agriculture Sciences, Xingcheng 125100, China; mayday0318143@163.com (B.Z.)
[2] College of Horticulture, China Agricultural University, Beijing 100193, China
* Correspondence: zszhouqrj@163.com

Abstract: Apple (*Malus domestica*) is an economically important fruit crop, but its production is affected by Glomerella leaf spot, a devastating disease caused by the fungal pathogen *Colletotrichum gloeosporioides*. MicroRNA (miRNA) is a kind of non-coding RNA that plays an important role in the process of plant–pathogen interactions. However, little is known about the miRNAs that influence apple resistance against *C. gloeosporioides*. A novel miRNA, *MIR396d-p3*, was identified through small RNA sequencing (sRNA-seq). Functional analyses revealed that *MIR396d-p3* negatively regulates apple resistance to *C. gloeosporioides*. In addition, *MdUGT89A2* and *MdRGA3* were confirmed as targets of *MIR396d-p3* using 5′ RACE and heterologous expression assays. We further found that overexpressing *MdUGT89A2* and *MdRGA3* induce apple disease resistance to *C. gloeosporioides*, while silencing of *MdUGT89A2* and *MdRGA3* reduces resistance to *C. gloeosporioides*. These results indicate that *MIR396d-p3* plays a role in the response to the infection of *C. gloeosporioides* through regulating the expressions of *MdUGT89A2* and *MdRGA3*. This research provides a new perspective on the interaction between apples and *C. gloeosporioides* and offers possible targets for resistance breeding.

Keywords: *MIR396d-p3*; apple glomerella leaf spot; *UGT89A2*; plant immune

check for updates

Academic Editor: Huali Xue

Received: 7 February 2025
Revised: 14 March 2025
Accepted: 22 March 2025
Published: 25 March 2025

Citation: Zhang, B.; Tang, J.; Ji, Z.; Du, Y.; Cong, J.; Zhou, Z. *MIR396d-p3* Negatively Regulates Apple Resistance to *Colletotrichum gloeosporioides* via *MdUGT89A2* and *MdRGA3*. *Horticulturae* **2025**, *11*, 351. https://doi.org/10.3390/horticulturae11040351

Copyright: © 2025 by the authors. Licensee MDPI, Basel, Switzerland. This article is an open access article distributed under the terms and conditions of the Creative Commons Attribution (CC BY) license (https://creativecommons.org/licenses/by/4.0/).

1. Introduction

Apple (*Malus domestica*) is a major fruit crop worldwide but suffers significant yield losses due to persistent fungal pathogens [1]. Apple glomerella leaf spot (GLS), caused by *Colletotrichum gloeosporioides* (*C. gloeosporioides*), leads to defoliation and a marked decline in apple yield [2]. The main varieties of apple in the world, such as "Golden Delicious" and "Gala", are universally susceptible to GLS, thereby exacerbating the impact of this disease [3]. High levels of humidity and temperature lead to recurrent outbreaks of GLS that affect both leaves and fruits [4]. Chemical control continues to be the predominant approach for managing apple GLS disease at this time, but treatments have negative repercussions, impacting environmental health and jeopardizing food safety. Deciphering the resistance mechanisms of apples against *C. gloeosporioides*, along with cultivating new resistant germplasm, would be a more effective approach.

MicroRNAs (miRNAs) are small non-coding RNAs that regulate gene expression post-transcriptionally by binding to target mRNAs and inhibiting their translation or promoting degradation [5]. Mounting evidence has revealed that miRNAs perform critical regulatory roles in plant–pathogen interactions [6]. In particular, miRNAs play vital regulatory roles in the response of apple to various fungal pathogens, such as *Botryosphaeria dothidea* [7–10],

Alternaria alternata [11–13], and *C. gloeosporioides* [14]. However, the precise mechanisms by which miRNAs mediate apple resistance to *C. gloeosporioides* are still not well understood. Specifically, the role of *miR396* in regulating apple resistance to *C. gloeosporioides* has not yet been reported, while the regulation of immune responses to pathogenic infections by *miR396* in Arabidopsis [15], rice [16], tomato [17], and soybean [18] has been documented.

UDP-glycosyltransferases (*UGTs*) are pivotal biotransformation enzymes that have developed across a wide range of living organisms, including bacteria, fungi, plants, and animals [19]. *UGTs* are essential for the glycosylation of small molecules [20]. This process can modify the homeostasis of these compounds by influencing their chemical activity, degradation, and distribution. *UGTs* are involved in various processes related to plant growth and defense response [21–23]. For example, *UGT73C7* is a pathogen-induced glycosyltransferase in Arabidopsis that enhances disease resistance by redirecting phenylpropanoid metabolism and upregulating the expression of the *SNC1* gene, a key component in plant immunity [21]. In addition, UDP-glucosyltransferase *HvUGT13248* is conferred type II resistance to Fusarium head blight (*FHB*) in barley by glucosylating the mycotoxin deoxynivalenol (*DON*) to its nontoxic form, DON-3-O-glucoside (*D3G*), and demonstrates that mutations in *HvUGT13248* increase susceptibility to *F. graminearum* infection [22]. Given these findings [21,22], we hypothesize that *UGTs* may play a pivotal role in apple resistance to *C. gloeosporioides*. However, there have been no reports on the study of *UGTs* in the disease resistance of apples.

Plant disease resistance genes (*R* genes) are the most recognized group of resistance gene analogs (*RGAs*), playing a vital role in sensing and defending against various plant pathogens [24]. This typical *R* gene structure usually comprises three domains: a leucine-rich repeat (LRR), a nucleotide-binding domain (NBD), and a signaling domain, which includes the Toll/IL-1 receptor (TIR), RESISTANCE TO POWDERY MILDEW 8 (RPW8), and the coiled-coil (CC) domain [25]. In addition, *R* genes and *RGAs* serve as essential genetic resources for managing plant diseases and offering immune protection against significant pathogen-related damage. Therefore, it is essential to dissect the role of *RGAs* in the resistance of apples to *C. gloeosporioides*.

This study used sRNA-seq technology to analyze how apple miRNA responds to the infection of *C. gloeosporioides*. At the same time, a novel miRNA, *MIR396d-p3*, is identified as the research object of this study. Then we predicted and verified through 5′ RACE and heterologous expression assays that *MdUGT89A2* and *MdRGA3* are direct targets of *MIR396d-p3.* To further confirm this regulatory relationship, expression profiling of *MIR396d-p3* and its target genes was detected in susceptible and resistant cultivars. In addition, we found that *MIR396d-p3* regulates resistance to *C. gloeosporioides* by modulating the expression of *MdUGT89A2* and *MdRGA3* through functional analyses. Taken together, this research provides a new perspective on the interaction mechanism between apples and *C. gloeosporioides*.

2. Material and Methods

2.1. Plant Material and Pathogen Cultures

The apple cultivars “Royal Gala” (abbreviated as “GL-3”) and “Fuji” (“FJ”) were maintained in vitro using Murashige and Skoog basal medium containing specific plant growth regulators: 0.6 mg·L^{-1} benzylaminopurine (BAP), 0.4 mg·L^{-1} α-naphthaleneacetic acid (NAA), and 0.2 mg·L^{-1} gibberellin A3 (GA3). The plant materials were grown at 25 ± 1 °C under controlled conditions and a 16/8 h light/dark cycle with a light intensity of 120 μmol m^{-2} s^{-1} in humidity-controlled chambers maintaining saturated moisture. For experimental standardization, in vitro-developed apple plantlets at 28 days of maturity were systematically selected as biological material for subsequent experiments.

Nicotiana benthamiana were sown in a mix (vermiculite, perlite, and soil in a 1:1:1 ratio). *N. benthamiana* plantlets were cultivated under controlled environmental conditions, including a temperature regime of 22 ± 1 °C, a 16/8 h light/dark cycle with a light intensity of 120 µmol m^{-2} s^{-1}, and 80% relative humidity.

The *C. gloeosporioides* strain W16, preserved in our laboratory, was grown on potato dextrose agar (PDA) medium at 28 °C for 3 days [26]. A sterilized toothpick was then employed to abrade the mycelial surface to promote sporulation. After an additional 4 days of incubation, we rinsed the mycelium and spores on the plate with sterile water. We filtered the resulting suspension through four layers of sterile gauze to remove mycelial fragments. We collected the filtrate containing spores and adjusted the spore concentration to 1×10^6 conidia·mL^{-1} for the subsequent experiments.

2.2. sRNA-Seqencing and Identification of Differentially Expressed microRNAs (DE-miRNAs)

To investigate whether miRNAs are involved in the response of apple plants to *C. gloeosporioides* infection, we performed sRNA-seq analysis using the susceptible cultivar "GL-3". Newly emerged apical leaves (3–4 leaves per plant) were inoculated with a conidial suspension of *C. gloeosporioides*. Samples were collected 24 h post-inoculation, with three bottles of leaves pooled as one biological replicate, and three independent biological replicates were subjected to sequencing analysis. Total RNA from "GL-3" plants, both inoculated with *C. gloeosporioides* and uninoculated controls, was extracted using a column method according to the method reported by Zhang et al. [27]. The quantification and purity evaluation of total RNA were performed with Nanodrop (Life Technologies, Carlsbad, CA, USA) and a Bioanalyzer 2100 (Agilent Technologies, Santa Clara, CA, USA). Subsequently, the small RNA libraries were assembled using the 5′-phosphate-dependent method and were sequenced on an Illumina HiSeq 2000/2500 platform [28].

The obtained raw data were selected by aligning them against various RNA databases, including the RFam database and the Repbase database, resulting in valid small RNA data for subsequent analysis [29]. In order to screen for differentially expressed miRNAs, we utilized *p*-values and fold change for selection. The specific criteria were $\log_2|(\text{fold change})| \geq 1$ and $p\text{-value} < 0.05$.

2.3. Bioinformatics Analysis

The target genes of candidate miRNA and the RNA secondary structure of candidate precursor miRNA were predicted using the psRNATarget web server [30] (https://www.zhaolab.org/psRNATarget/, accessed on 21 March 2025) and the UNAFold Web Server (http://www.unafold.org, accessed on 21 March 2025), respectively. To understand how many plant species contain candidate miRNA families and the evolutionary relationship between candidate miRNA and the reported candidate miRNA family in apple, we downloaded all relevant information from the miRBase database. Meanwhile, we used MEGA_12.0.10 software to construct a phylogenetic tree about candidate precursor miRNA.

Similarly, the promoter sequence of candidate miRNA was obtained from the GDR database by aligning it with the apple genome sequence [28], and cis-acting elements in the promoter were analyzed using the PlantCARE web server (https://bioinformatics.psb.ugent.be/webtools/plantcare/html/, accessed on 20 January 2025). Finally, visualization of the results was performed using TBtools v2.061 [31].

2.4. Rapid Amplification of cDNA Ends Assay

Total RNA was obtained as described above. First strand cDNA was synthesized at 42 °C for 90 min and at 70 °C for 15 min using 5′ TS Oligo. Then, rapid amplification of cDNA ends (RACE) was conducted using the 5′ GSP provided in the HiScript-TS 5′/3′ RACE Kit. Nested PCR was then performed for multiple rounds of amplification to obtain

positive bands. Subsequently, 24 randomly selected clones were sent for sequencing to a company.

2.5. Plasmid Construction

35S: *MIR396d-p3* construct. The sequence of the *MIR396d-p3* precursor was introduced into the pFGC5941 vector at the NcoI/BamHI site.

35S: STTM-*MIR396d-p3* construct. A fragment containing two partially complementary sequences of *MIR396d-p3*, separated by a 48-base pair short spacer, was artificially synthesized and introduced into the pFGC5941 binary vector.

35S: *MdUGT89A2*-GUS construct. The full coding sequence of *MdUGT89A2*, excluding the stop codon, was introduced into the pFGC5941 vector at the NcoI/BamHI site.

35S: *MdRGA3*-GUS construct. The complete coding sequence of *MdRGA3*, without the stop codon, was inserted into the pFGC5941 binary vector at the NcoI/BamHI site.

35S: *MdUGT89A2* construct. The coding sequence of *MdUGT89A2* was introduced into the pFGC5941 binary vector.

35S: *MdRGA3* construct. The gene sequence of *MdRGA3* was cloned into the pFGC5941 binary vector.

RNAi construct. Two fragments with the sense and antisense sequences of *MdUGT89A2* and *MdRGA3* were inserted into the flanking regions of the pFGC5941 intron, respectively.

2.6. Agrobacterium-Mediated Transient Transformation

Transformation of all recombinant constructs was performed in *Agrobacterium tumefaciens* GV3101 cells. A single colony of *Agrobacterium* was grown in LB liquid medium containing rifampin (50 $\mu g \cdot mL^{-1}$) and kanamycin (50 $\mu g \cdot mL^{-1}$). Subsequently, the bacteria were suspended in a buffer solution composed of 10 mM $MgCl_2$, 10 mM MES, and 100 μM acetosyringone, with a pH adjusted to 5.6. The suspension was incubated at 25 °C in the dark for 2 h prior to its use in transient transformation experiments.

2.7. Histochemical Staining and GUS Activity Quantification

GUS staining assay was conducted on *N. benthamiana* infiltrated leaves according to previously reported methods [32]. The *N. benthamiana* leaves utilized for histochemical GUS staining were subjected to an incubation at 37 °C overnight. Subsequently, they were placed in a series of ethanol solutions with increasing concentrations (30%, 50%, and 70%) to facilitate visualization.

To further quantify GUS activity, the fluorometric 4-methylumbelliferyl-β-D-glucuronide (*MUG*) method was employed. The specific method should be carried out in accordance with the GUS gene quantitative detection Kit (Coolaber Science & Technology, Beijing, China). A unit of GUS activity is characterized by the production of 1 nM of 4-methylumbelliferone per minute for each milligram of soluble protein. In each treatment, 10 leaves corresponding to each construct were collected for detection.

2.8. RT-qPCR Assay

To validate the expression patterns of miRNAs and their target genes, total RNA was extracted using a column-based method at 4 d post-transfection. For temporal profiling of miRNA expression, additional samples were harvested at 24 and 72 h post-transfection, followed by RNA extraction using the same protocol. First-strand cDNA was generated through the HiScript II 1st Strand cDNA Synthesis Kit (Vazyme Biotech Co., Ltd., Nanjing, China). The expression level of mature *MIR396d-p3* was analyzed using stem-loop real-time quantitative PCR, with 5S rRNA and *MdActin* serving as internal controls. RT-qPCR was conducted in accordance with the instructions provided for ChamQ SYBR qPCR Master

Mix using CFX Connect TM Real-Time System (BIO-RAD, Hercules, CA, USA). The $2^{-\Delta\Delta CT}$ method was used to calculate relative expression levels of the corresponding genes [33].

To quantify fungal biomass, fungal and plant DNA extraction kits (Sangon Biotech, Shanghai, China) were employed to isolate *C. gloeosporioides* DNA and apple genomic DNA from leaf samples collected at 48 h post-inoculation, respectively. Subsequently, the fungal *Cgβ-Tubulin* gene and the apple *MdActin* gene were selected as internal reference genes for biomass quantification. Utilizing the same RT-qPCR reaction conditions and calculation procedures as described for the RT-qPCR assay, biomass data were obtained.

2.9. Statistical Analysis

The statistical analyses were implemented using GraphPad Prism 10 software. The data are expressed as the mean ± standard error (SE). One-way ANOVA followed by Tukey's test ($p < 0.05$) was used to analyze significant differences.

3. Results

3.1. Analysis of Apple Small RNA Sequencing Response to C. gloeosporioides

To investigate whether miRNAs of apple are involved in the response to *C. gloeosporioides* infection, sRNA-seq was conducted, and the clean data were obtained. First, we removed miRNAs mapped to two positions of the same precursor on the genome; the unique count of candidate RNAs was obtained. The length distribution analysis of the above miRNAs is shown in Figure S1B. According to Figure S1B, we found that the most abundant small RNAs produced in the leaves of "GL-3" apple were 24 nt in length, followed by 23 nt, 22 nt, and 21 nt. Additionally, 284 conserved miRNAs belonged to 47 miRNA families (Figure S1A). Among these families, *miR156* is the largest, with a total of 37 members, followed by the *miR166*, *miR167*, and *miR159* families, which contain 17, 15, and 14 members, respectively. Furthermore, there are some miRNA families with only one member, such as *miR1510*, *miR4243*, *miR7533*, *miR7125*, and *miR8775*.

To better understand the DE-miRNAs and their target genes, we performed GO (Gene Ontology) enrichment analysis and KEGG (Kyoto Encyclopedia of Genes and Genomes) analysis on the predicted target genes. The results are shown in Figure S1C,D. According to Figure S1C,D, the target genes of the DE-miRNAs are mainly enriched in biological processes such as defense response, regulation of transcription by RNA polymerase II, cell differentiation, cellular response to iron ions, and signal transduction. The KEGG analysis results indicate that the target genes of the DE-miRNAs play significant roles in pathways related to spliceosomes, plant–pathogen interactions, starch and sucrose metabolism, and *MAPK* signaling. Based on the GO and KEGG analyses, it can be concluded that these target genes of DE-miRNAs play important roles in the response of "GL-3" apple leaves to *C. gloeosporioides* infection.

3.2. Validation of sRNA-Seq Data Using RT-qPCR

To investigate the credibility of sRNA-seq, the expression profiles of nine differentially expressed miRNAs (DE-miRNAs), including *miR395a*, *MIR10994-p5_1ss6TC*, *MIR10986-p3_1ss21GT*, *MIR2916-p5_1ss5AG*, *MIR390a-p3*, *miR156e_R+1*, *MIR395c-p5*, *miR167a*, and *PC-3p-4885_278*, were detected through RT-qPCR at 0 h, 24 h, and 72 h post-infection. As shown in Figure 1, RT-qPCR demonstrated that *miR395a* exhibited a significant increase as the infection time increases; this trend is consistent with the sRNA-seq data. Similarly, the expression levels of *MIR10994-p5_1ss6TC* and *MIR10986-p3_1ss21GT* also show an increase with the increase in the infection time, and the expression levels are also increasing. Interestingly, most of these miRNAs were upregulated at 24 h or 72 h, except *miR167a* and *PC-3p-4885_278*. In general, the results from RT-qPCR aligned well with the sRNA-seq data.

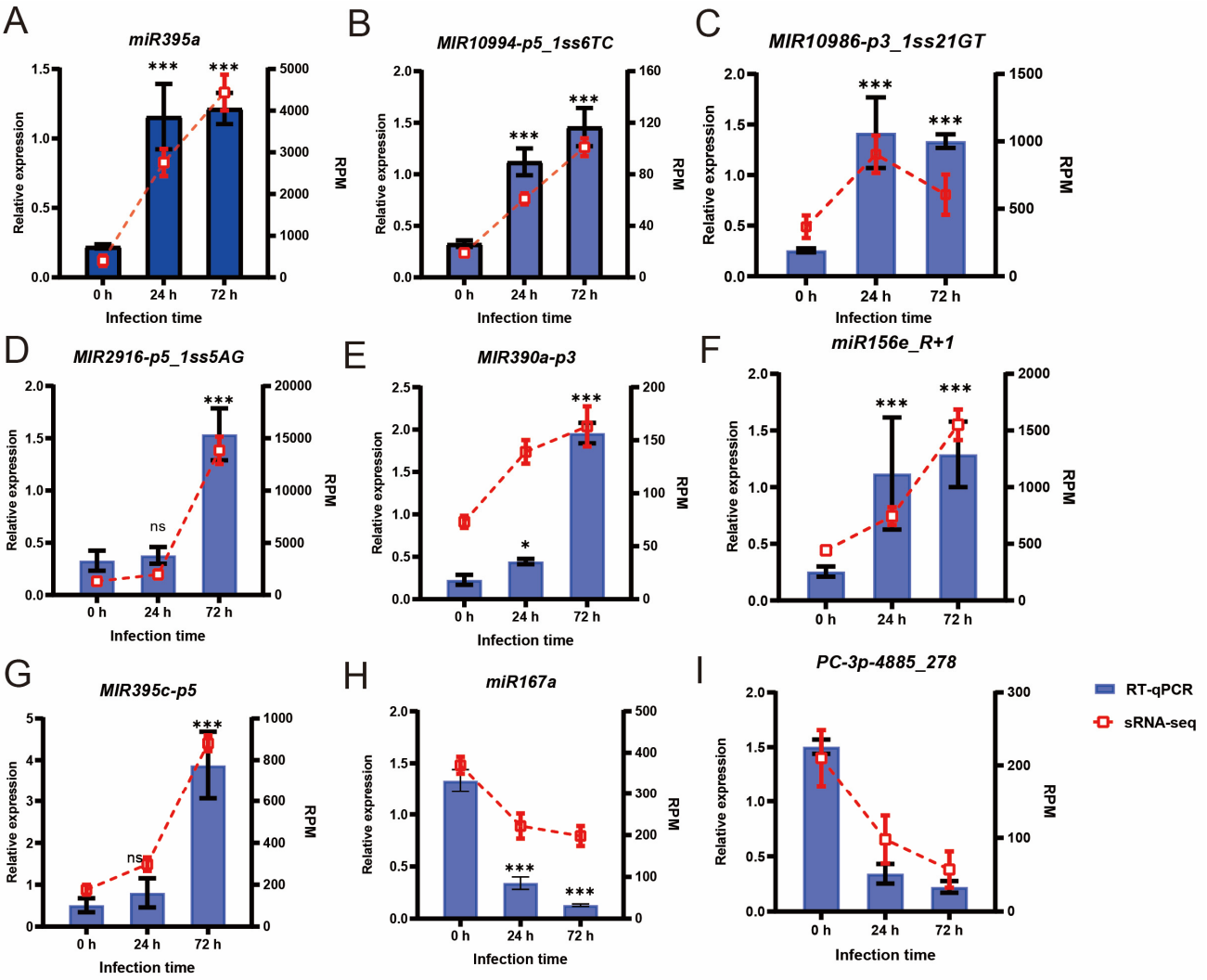


Figure 1. RT-qPCR validation of differentially expressed miRNA (DE-miRNA) expression in apple leaves following *Colletotrichum gloeosporioides* infection. Comparison with sRNA-seq (miRNA) and RNA-seq (transcriptome) data is shown. Blue bars represent qRT-PCR expression levels; red lines indicate RNA-seq and sRNA-seq derived expression. Results are expressed as mean ± SD (n = 3). Statistical significance was determined by one-way ANOVA followed by Tukey's post-hoc test. * ($p < 0.05$), and ***($p < 0.001$) indicate significant differences. ns: not significant.

3.3. Identification and In Silico Analysis of miRNA Response to C. gloeosporioides

To investigate the possible miRNAs response to *C. gloeosporioides*, we selected a miRNA of particular interest, *MIR396d-p3*, based on *p*-values and fold change (FC). This is because *miR396* is a highly conserved small RNA molecule that has been identified in a wide range of plant species. According to the miRBase database (version 22.1), information about the *miR396* family has been found in 52 plant species (Figure S2). *miR396* may hold significant research value. Meanwhile, *MIR396d-p3* expression significantly increased after 24 h of infection, indicating its response to *C. gloeosporioides* infection (Figure 2A). First, we predicted the RNA secondary structure of the *MIR396d-p3* precursor through the UNAFold Web Server. The results were shown as Figure 2B: the *MIR396d-p3* precursor can form a secondary structure, indicating that the miRNA precursor may be stable and capable of being successfully processed into mature miRNA. Meanwhile, by aligning with the apple genome, it was found that the *MIR396d-p3* precursor is located between positions 2032169 and 2032271 on chromosome 2 (Figure 2C).

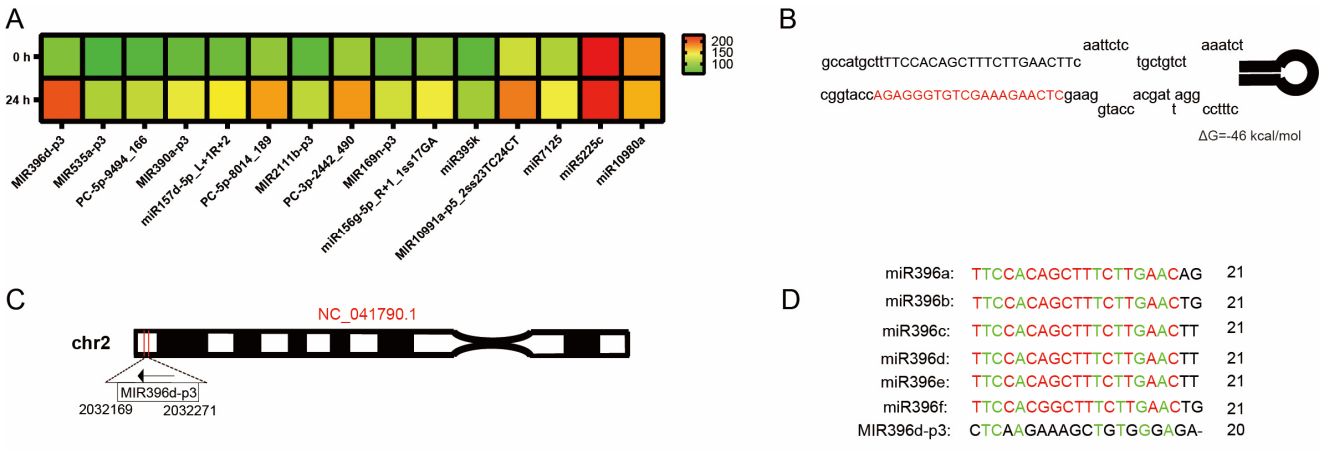


Figure 2. Identification and in silico analysis of *MIR396d-p3*. (**A**) The heatmap showing the *MIR396d-p3* was identified post-infection. (**B**) The secondary structure of a *MIR396d-p3* precursor sequence predicted through RNA-fold web service, with the free-energy value indicated. (**C**) The location of *MIR396d-p3* precursor sequence on chromosome 2 in the genome, with the corresponding NCBI accession number (NC_041790.1) marked. (**D**) Sequence alignment of *mdm-miR396* sequences. Red representative almost identical except for one base, green represents the same base.

To understand which environmental factors might influence *MIR396d-p3*, we predicted the cis-acting elements in the promoter region of the *MIR396d-p3* precursor. The results, shown in Figure S3, indicate that factors such as pathogen infection, light, jasmonic acid, and abscisic acid can influence its expression. In addition, by comparing with the existing apple *miR396* in the miRBase database, we found that apple *miR396* is highly conserved, despite some genetic evolution observed in *MIR396d-p3* (Figures 2D and S4).

3.4. MIR396d-p3 Cleaves MdUGT89A2 and MdRGA3 Transcripts

To screen the target genes of *MIR396d-p3*, we conducted a series of computational predictions through psRNATarget. As shown in Table S1, eight target genes were selected based on their predicted interactions with *MIR396d-p3*, including 1-aminocyclopropane-1-carboxylate synthase 7-like, transcription factor *bHLH111*-like, receptor protein kinase *ZmPK1*, *WAT1*-related protein, disease resistance protein *RGA3*, UDP-glycosyltransferase 89A2 (*UGT89A2*), peroxidase 29, and serine acetyltransferase. Next, we conducted 5′ RACE experiments on these eight target genes and found that only *UGT89A2* and *RGA3* interacted with *MIR396d-p3* (Figure 3A). To further clarify that *MIR396d-p3* can cleave *MdUGT89A2* and *MdRGA3* transcripts, we performed heterologous expression in *N. benthamiana*. First, we constructed 35S:*MIR396d-p3* and the corresponding 35S-*UGT89A2*:GUS, 35S-*RGA*:GUS using the Cloning Kit V2 (Figure 3B). Then, we co-injected them into *N. benthamiana* to assess their expression and detected GUS activity to determine if they interacted. Meanwhile, 35S:GUS served as a positive control, and 35S:*MIR396d-p3* served as a negative control. As shown in Figure 3D, 35S-*UGT89A2*:GUS and 35S-RGA:GUS did not show significant differences compared to 35S:GUS; however, when they were co-expressed with *MIR396d-p3*, their expression levels were significantly reduced, indicating that *MIR396d-p3* can cleave *MdUGT89A2* and *MdRGA3* transcripts. GUS staining also exhibited a similar phenotype (Figure 3C).

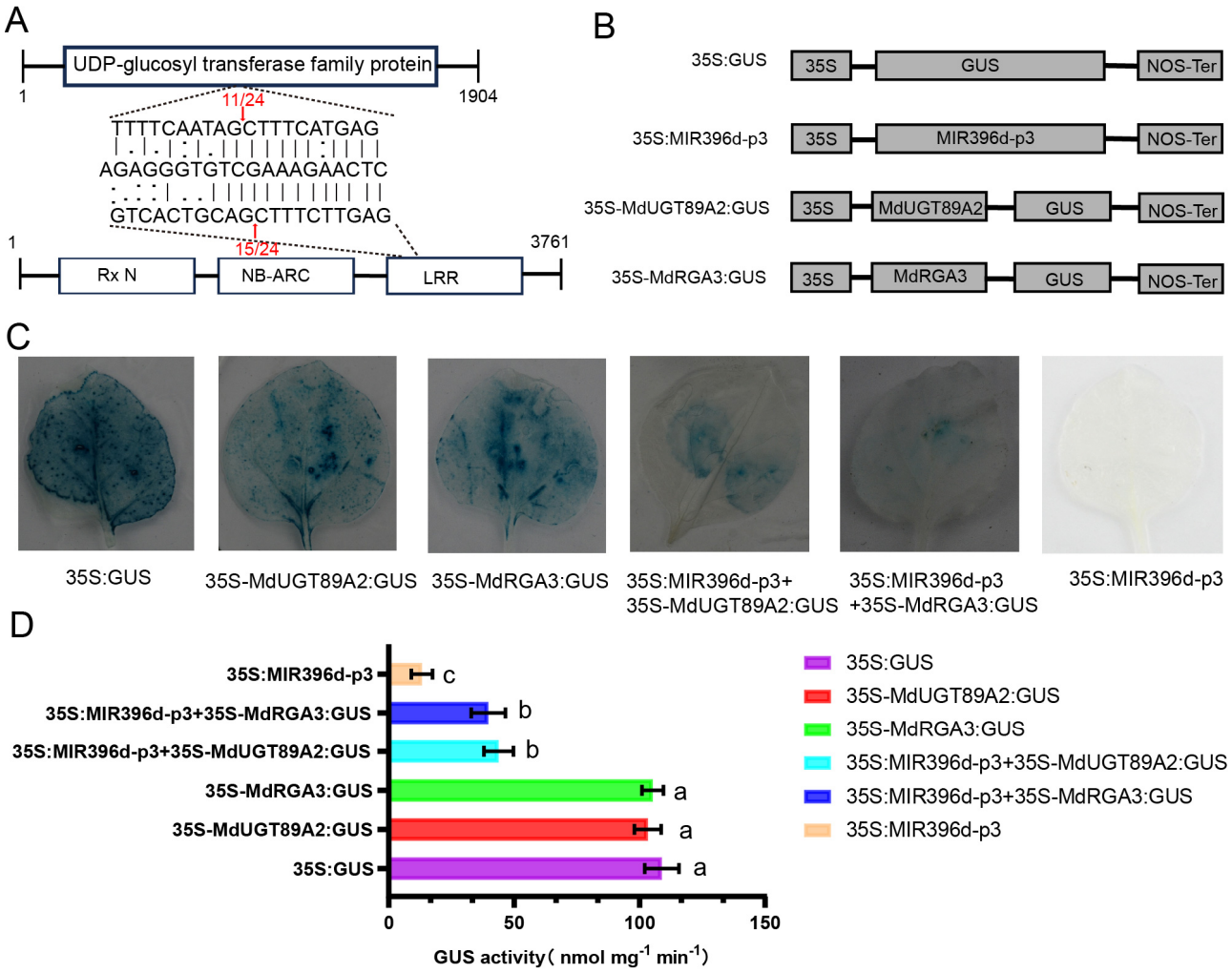


Figure 3. *MIR396d-p3* cleaves *MdUGT89A2* and *MdRGA3* transcripts. (**A**) 5′ RACE identified the cleavage site of the predicted *MIR396d-p3* target. The arrow denotes the cleavage site, and the numbers above indicate the frequency of cleavage at that site in independent clones. (**B**) Schematic diagrams of constructs used for co-transformation of *Nicotiana benthamiana*. (**C**) Histochemical GUS staining of *N. benthamiana* leaves 3 d post-infiltration with the indicated constructs. (**C**) Representative image from three independent experiments. (**D**) Quantification of GUS activity in *N. benthamiana* leaves transiently expressing the indicated constructs. Data represent means ± SD of three technical replicates. Different letters indicate significant difference $p < 0.05$ (one-way ANOVA followed by post hoc Tukey test). All data are shown as means ± SD (n = 9).

To assess the expression pattern of *MIR396d-p3* and its target genes *MdUGT89A2* and *MdRGA3* in the susceptible variety "GL-3" and the resistant variety "FJ", RT-qPCR assay was conducted at 0, 24, and 72 h post-*C. gloeosporioides* infection. As shown in Figure 4, the expression level of *MIR396d-p3* was significantly upregulated in"GL-3", while *MdUGT89A2* and *MdRGA3* were strikingly downregulated. Meanwhile, the expression level of *MIR396d-p3* in "FJ" continuously decreases as the infection time increases, while *MdUGT89A2* and *MdRGA3* were upregulated. Collectively, *MIR396d-p3* can negatively regulate the expression of *MdUGT89A2* and *MdRGA3*.

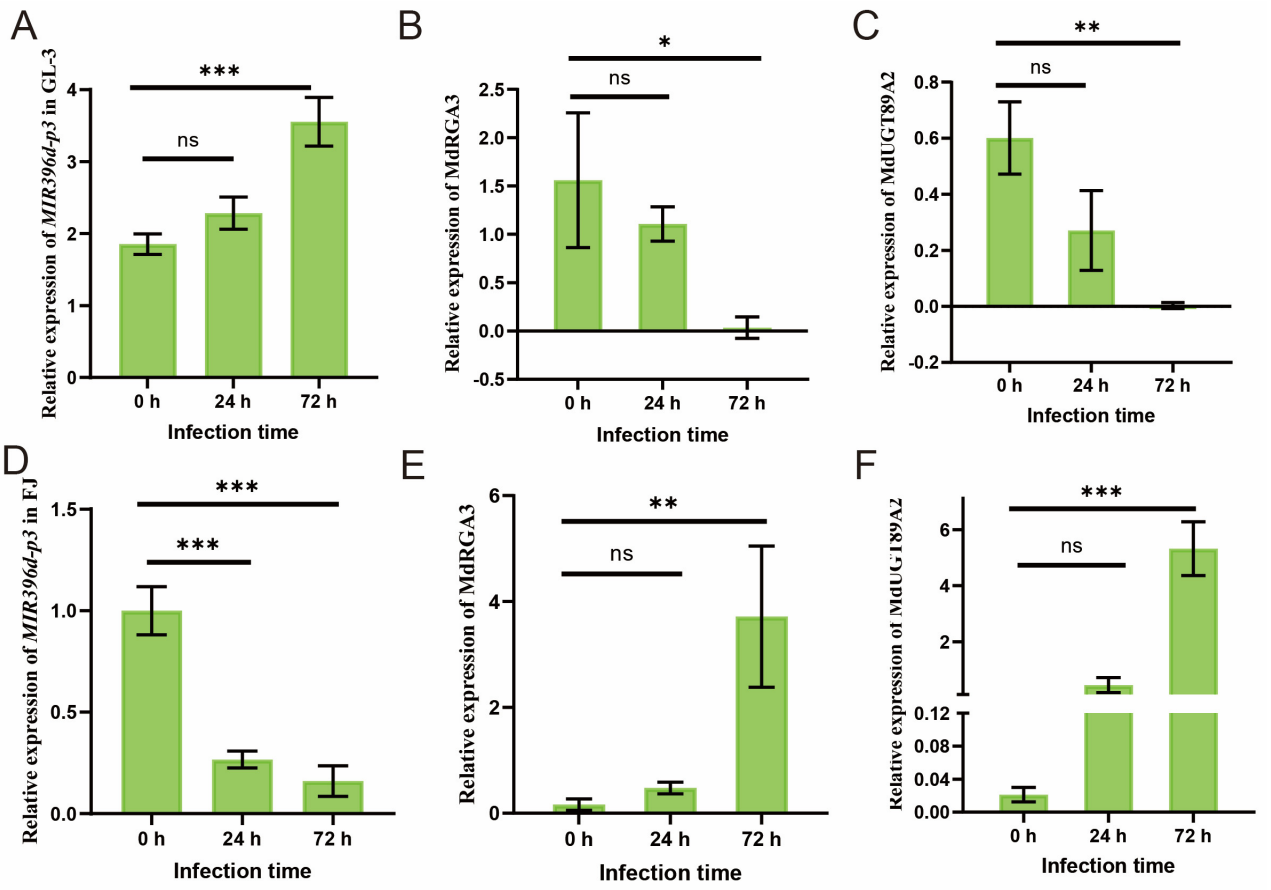


Figure 4. Analyses of expression patterns of *MIR396d-p3* and its target genes *MdUGT89A2* and *MdRGA3* in the apple response to *Colletotrichum gloeosporioides* infection. Expression analysis of mature *MIR396d-p3* in "GL-3" (**A**) and "FJ" (**D**) apple leaves at the indicated time points after inoculation with *C. gloeosporioides* using stem-loop RT-qPCR. Relative expression of *MdRGA3* (**B**) and *MdUGT89A2* (**C**) in "GL-3" apple leaves at 0, 24, and 72 h post-*C. gloeosporioides* infection (qRT-PCR). Relative expression of *MdRGA3* (**E**) and *MdUGT89A2* (**F**) in "FJ" apple leaves at 0, 24, and 72 h post-*C. gloeosporioides* infection (qRT-PCR). A one-way ANOVA was performed, followed by a Tukey's test (a post-hoc test used for multiple comparisons after a significant ANOVA result). Significant differences are marked with asterisks: * $p < 0.05$, ** $p < 0.01$, *** $p < 0.001$. ns: not significant.

3.5. Responsiveness of MIR396d-p3 to C. gloeosporioides Infection

To investigate the involvement of *MIR396d-p3* in the apple's response to *C. gloeosporioides*, we cloned the *MIR396d-p3* precursor into the pFGC5941 vector to construct the *MIR396d-p3* overexpression vector (Figure 5A). Then the overexpressed constructed vector was transformed into the resistant apple cultivar "FJ" via *Agrobacterium*-mediated transformation. The expression level of *MIR396d-p3* was assessed through RT-qPCR at 4 d post-inoculation. As shown in Figure 5B, the expression level of *MIR396d-p3* was significantly higher in the *MIR396d-p3* overexpression plants compared to wild-type "FJ" and the pFGC5941 EV control (EV).

Disease lesion areas were measured at 2 d post-*C.gloeosporioides* inoculation. The OE-*MIR396d-p3* plants exhibited significantly larger lesions compared to "FJ" and EV (Figure 5C,D). In addition, *C. gloeosporioides* biomass in the OE-*MIR396d-p3* plants was significantly higher than in the "FJ" and EV plants (Figure 5E). Based on these results, we therefore predicted that the *MIR396d-p3* is involved in the apple resistance response to *C. gloeosporioides*.

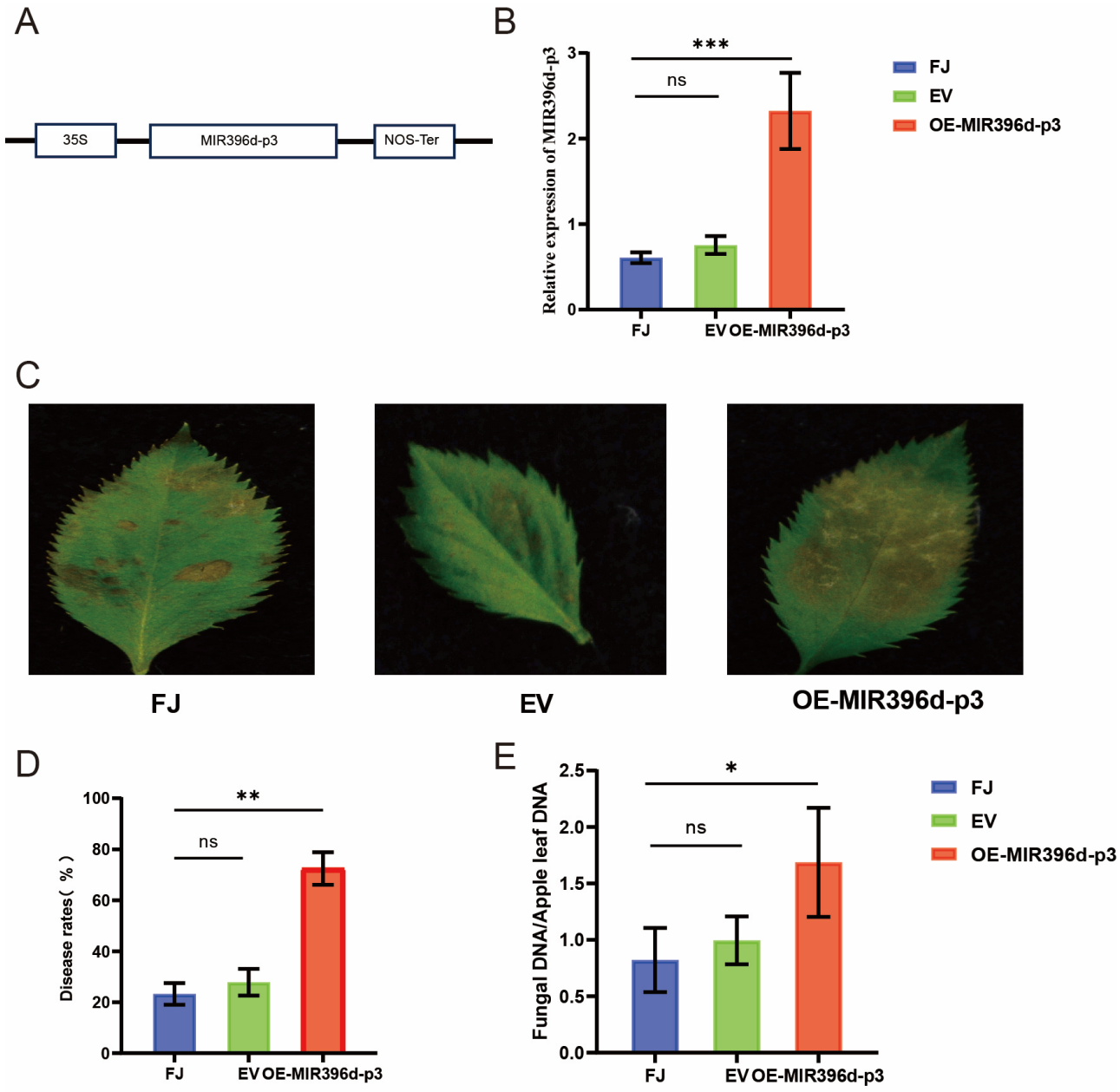


Figure 5. Overexpression of *MIR396d-p3* negatively regulates the resistance of apple to *C. gloeosporioides*. (**A**) Schematic diagrams of constructs used for *MIR396d-p3* overexpression. (**B**) The constitutive expression of mature *MIR396d-p3* (**B**) in non-infiltrated leaves and leaves infiltrated with different constructs by RT-qPCR analysis. (**C**) Representative symptoms in "FJ" leaves infected with *C. gloeosporioides*. The image is a photograph taken after inoculation at 48 h. (**D**) Percentage of infected "FJ" leaves at 48 hpi in different disease level classifications. (**E**) Relative biomass of *C. gloeosporioides* determined by quantitative PCR in infected leaves sampled at 48 hpi. Statistical significance was assessed via one-way ANOVA followed by Tukey's post-hoc test for multiple comparisons. Asterisks denote significant differences (* represent $p < 0.05$, ** represent $p < 0.01$, *** represent $p < 0.001$). ns: not significant.

To further explore the function of *MIR396d-p3* during the *C. gloeosporioides* infection, we constructed an *MIR396d-p3* silencing (STTM-*MIR396d-p3*) vector using STTM technology (Figure 6A). To evaluate the efficiency of silence, the STTM-*MIR396d-p3* vector was introduced into the susceptible apple cultivar "GL-3" via *Agrobacterium*-mediated transformation. We found that the expression level of *MIR396d-p3* was significantly reduced in STTM-*MIR396d-p3* plants, indicating that the *MIR396d-p3* is successfully silencing

(Figure 6B). Subsequently, these leaves were inoculated with *C. gloeosporioides*. After 2 days of inoculation, disease lesion areas were counted. Compared to the "GL-3" and EV plants, the STTM-*MIR396d-p3* plants displayed significantly reduced lesion areas (Figure 6C,D). The reduced *C. gloeosporioides* biomass in STTM-*MIR396d-p3* plants, quantified by RT-qPCR, further supports the observed effect that *MIR396d-p3* silencing enhances apple resistance to *C. gloeosporioides*. These findings strongly indicate *MIR396d-p3* negatively affects resistance to *C. gloeosporioides*.

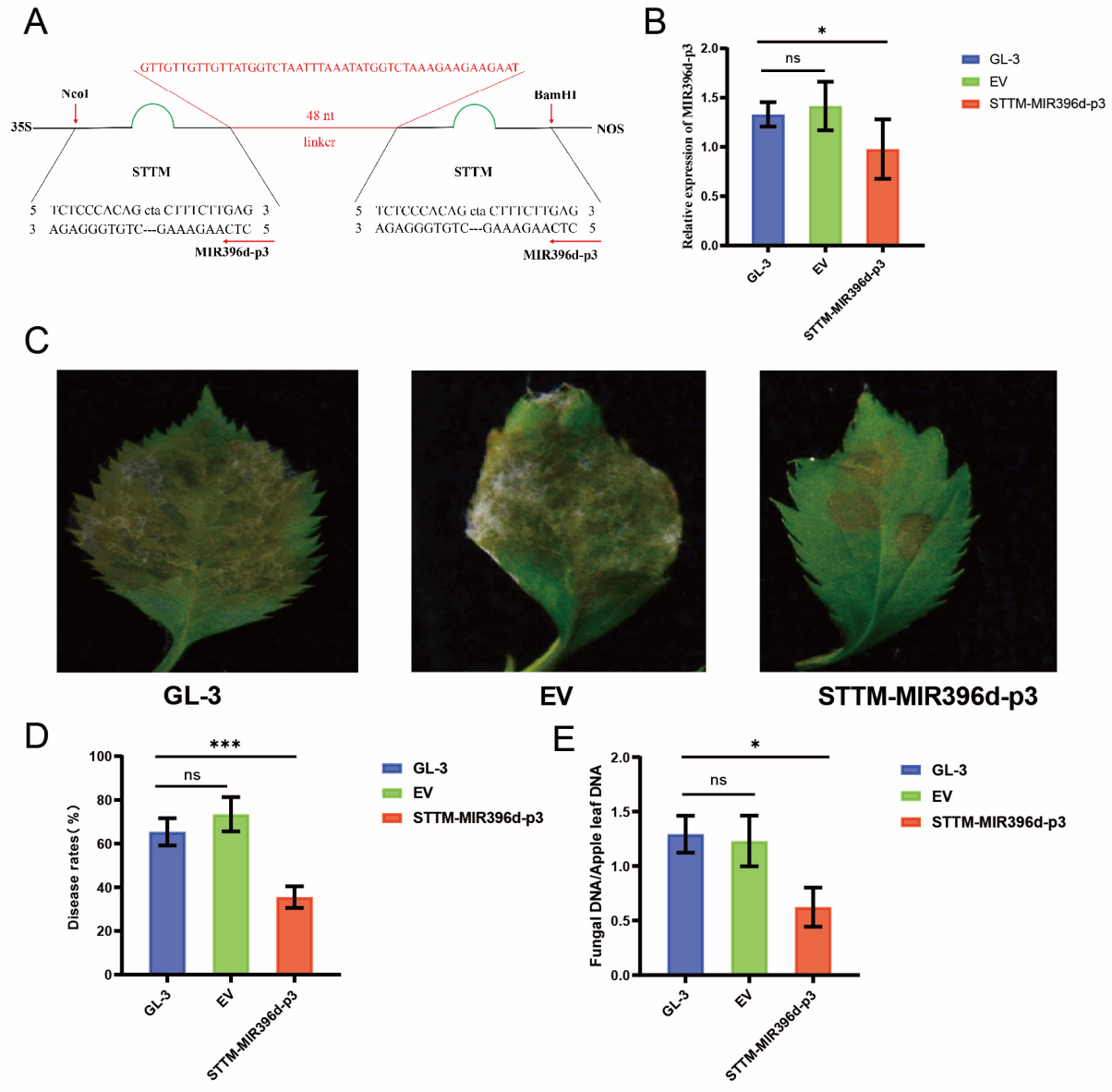


Figure 6. The *C. gloeosporioides* resistance of STTM-*MIR396d-p3* apple "GL-3" leaves. (**A**) Schematic structure of the construct for silencing *MIR396d-p3*. Relative expression levels of (**B**) *MIR396d-p3* in transiently transformed leaves of STTM-*MIR396d-p3*, "GL-3", and empty vector (EV) controls. Photographs of representative leaves with median lesion diameter in STTM-*MIR396d-p3*, "GL-3", and EV controls at 48 h after inoculation with *C. gloeosporioides* (**C**) are shown. (**D**) Determination of lesion diameter for different transformants inoculated with *C. gloeosporioides* were determined and analysed in STTM-*MIR396d-p3*, "GL-3", and EV plants. (**E**) Relative biomass of *C. gloeosporioides* was determined by qPCR. Statistical significance was assessed by one-way ANOVA with Tukey's post-hoc test. Significant differences are indicated by asterisks: * ($p < 0.05$), *** ($p < 0.001$). ns: not significant.

3.6. *MdUGT89A2 and MdRGA3 Are Involved in the Resistance to C. gloeosporioides in Apple*

We next examined the impact of *MdUGT89A2* and *MdRGA3* on apple's resistance to *C. gloeosporioides*. Full-length *MdUGT89A2* and *MdRGA3* sequences were amplified and cloned into the pFGC5941 vector to generate overexpression constructs (Figure S5). The construct was subsequently introduced into "GL-3" by *Agrobacterium*-mediated infiltration. RT-qPCR analysis confirmed successful overexpression of *MdUGT89A2* and *MdRGA3* in the OE-*MdUGT89A2* and OE-*MdRGA3* plants at 4 d post-transformation, respectively (Figure 7A). Lesion areas were measured 2 days following *C. gloeosporioides* inoculation. The OE-*MdUGT89A2* and OE-*MdRGA3* plants displayed a significantly reduced lesion area compared with the "GL-3" and EV plants. This similar result was further confirmed by the relative biomass (Figure 7D). These results indicated *MdUGT89A2* and *MdRGA3* positively regulate apple resistance to *C. gloeosporioides*.

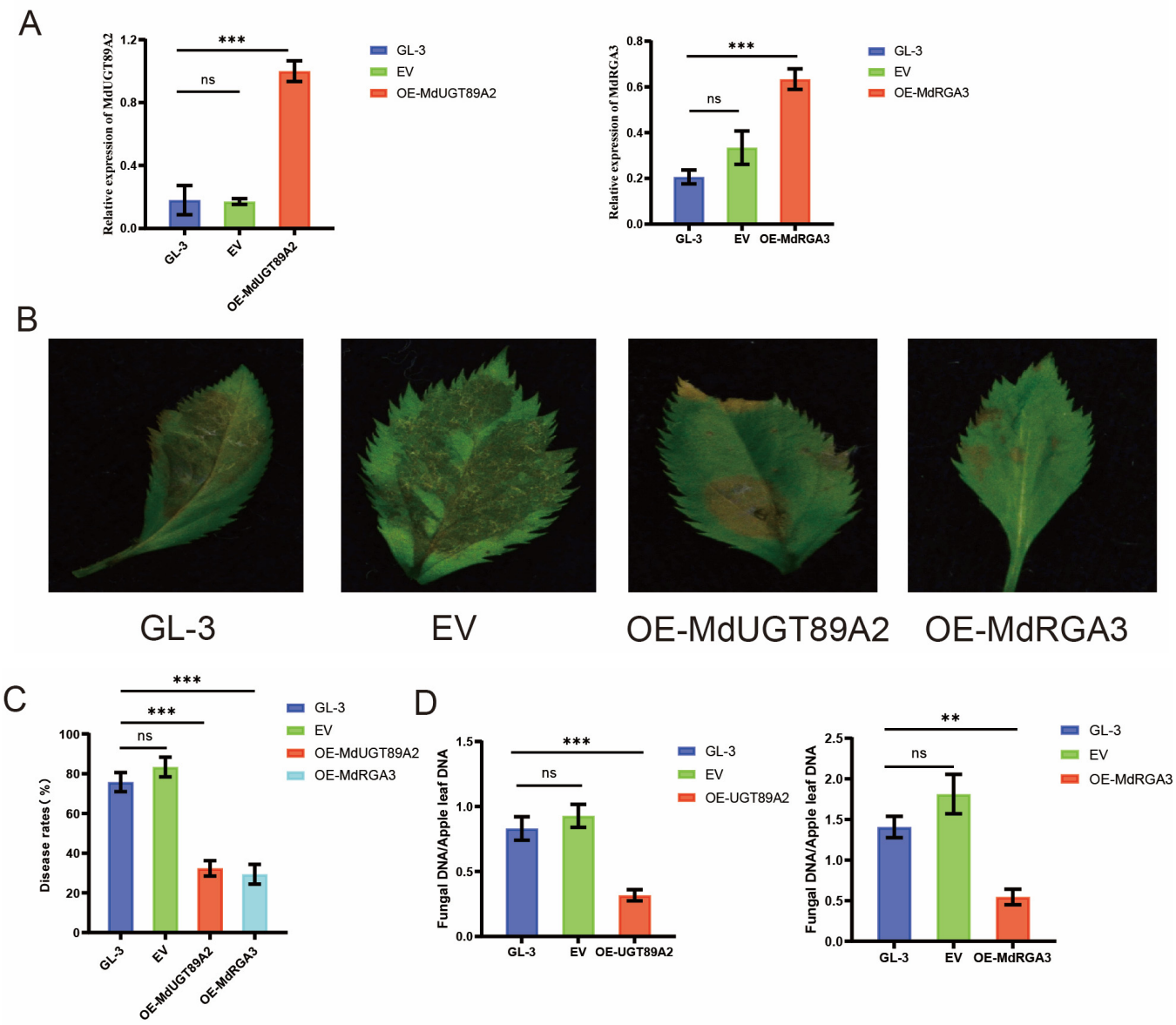


Figure 7. Transient overexpression (OE) of *MdUGT89A2* and *MdRGA3* enhances resistance to *C. gloeosporioides*. (**A**) Relative expression levels of the target genes in different plant lines ("GL-3", EV, OE-*MdUGT89A2*, OE -*MdRGA3*). Error bars represent standard deviations, and significance levels are indicated by asterisks (** indicated $p < 0.01$, *** represented $p < 0.001$, ns: not significant). (**B**) Phenotypes

of leaves from different plant lines, showing the differences in disease-related symptoms. (**C**) Disease severities of different plant lines, expressed as a percentage. Error bars represent standard deviations, and significance levels are indicated by asterisks. (**D**) Quantification of fungal DNA in different plant lines, indicating the accumulation of fungi. Statistical significance (one-way ANOVA, Tukey's post-hoc): ** $p < 0.01$, *** $p < 0.001$.

We used RT-qPCR to detect the expression level of *MdUGT89A2* and *MdRGA3* in the corresponding RNAi-silenced plants and found that *MdUGT89A2* expression was reduced by approximately ~76.74%, while *MdRGA3* expression was reduced by ~69.2%, relative to control plants (Figure 8A). Following inoculation with *C. gloeosporioides*, the lesion size was assessed on RNAi-*MdUGT89A2*, RNAi-*MdRGA3*, "FJ", and EV plants at 2 d post-inoculation. Silencing of *MdUGT89A2* and *MdRGA3* resulted in significantly larger lesions compared to "FJ" and EV plants. Consistent with the larger lesion sizes, *C. gloeosporioides* biomass was significantly elevated in plants with RNAi-mediated silencing of *MdUGT89A2* and *MdRGA3* (Figure 8D). Collectively, *MdUGT89A2* and *MdRGA3* function as positive regulators of apple resistance to *C. gloeosporioides*.

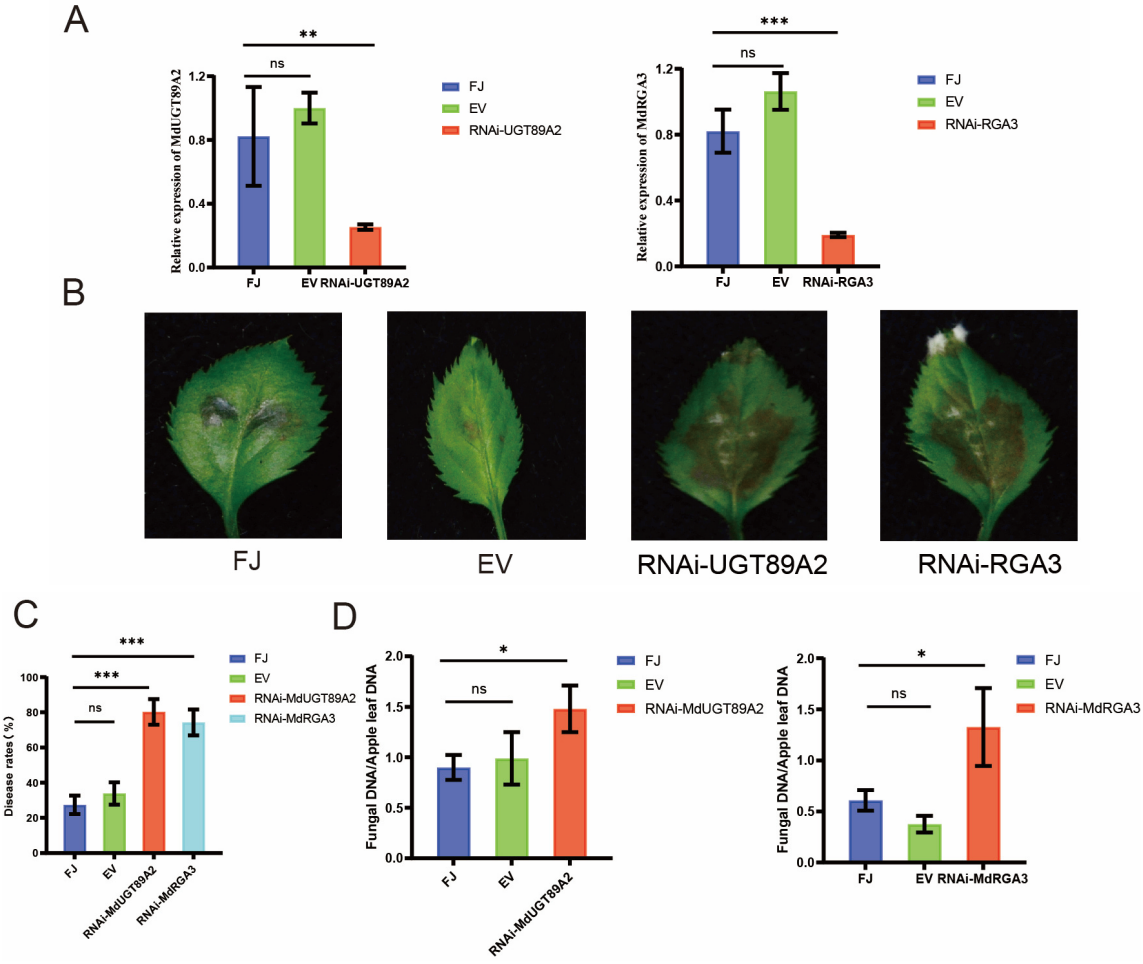


Figure 8. Silencing *MdUGT89A2* and *MdRGA3* comprises disease resistance against *C. gloeosporioides*. (**A**) The expression of the three treatments "FJ", EV, RNAi-*MdUGT89A2*, and RNAi-*MdRGA3* was detected using RT-qPCR. (**B**) Four days after *Agrobacterium* injection, "FJ", EV, RNAi-*MdUGT89A2*, and RNAi-*MdRGA3* were inoculated with *C. gloeosporioides*. These phenotypes as well as lesion area two days after inoculation with *C. gloeosporioides*. (**C**) Lesion area was analyzed statistically as shown. (**D**) Relative *C. gloeosporioides* biomass was determined by RT-qPCR. Comparisons between groups were analyzed using one-way ANOVA and Tukey's post-hoc test. Asterisks mark significant differences: * ($p < 0.05$), ** ($p < 0.01$), *** ($p < 0.001$). ns: not significant.

4. Discussion

In this study, we investigated the role of microRNA (miRNA) in apple's response to *C. gloeosporioides*, the causal agent of GLS. Through sRNA sequencing, a novel miRNA, *MIR396d-p3*, was identified. Bioinformatic analysis of *MIR396d-p3* target genes and its promoter region indicated that *MIR396d-p3* may regulate key aspects of biological processes, including plant defense, signal transduction, plant–pathogen interactions, and light-mediated responses. Previous studies have reported the involvement of Arabidopsis *miR396* in mediating immune responses against fungal pathogens [15]. Therefore, we hypothesize that *MIR396d-p3* may also play a role in apple's defense against *C. gloeosporioides* infection.

MiR396-mediated cleavage of growth-regulating factors (*GRFs*) has been observed in diverse plant species, including switchgrass (*Panicum virgatum*) [34], rice (*Oryza sativa*) [16], Arabidopsis (*Arabidopsis thaliana*) [15], and poplar (*Populus* spp.) [35], tomato (*Solanum lycopersicum*) [36], and soybean (*Glycine max*) [18]. The *miR396-GRF* regulatory module represents a novel and efficient mechanism for modulating plant growth, development, and responses to environmental stresses. Interestingly, our integrated analysis of bioinformatics prediction and experimental validation identified two novel *MIR396d-p3* target genes, *MdUGT89A2* and *MdRGA3*. These previously unreported targets significantly advance our understanding of the *miR396*-mediated regulatory mechanisms underlying plant stress responses.

Plants have independently evolved UDP-glycosyltransferases (*UGTs*) with specific substrate specificities, enabling fine-tuned regulation of defensive secondary metabolites and thereby resisting pathogen infection. They work by attaching glucose to various substances, such as toxins, hormones, and other metabolites [20]. This process usually helps detoxify harmful substances, protecting the plant from damage. In relation to fungal pathogens, *UGTs* can alter mycotoxins produced by the fungus, making them less harmful and impeding the pathogen's ability to cause infection [23]. We found that overexpressing *MdUGT89A2* enhances resistance to *C. gloeosporioides*. This discovery opens new avenues for developing disease-resistant apple varieties by manipulating this crucial regulatory pathway. However, we have not yet studied the potential substrates of *UGT*s and what immune responses are activated in response to pathogen infection. On the other hand, *MdRGA3* belongs to the family of *R* genes, which are essential for recognizing and defending against pathogen attacks [37,38]. Overexpression of *MdRGA3* significantly increases the resistance to *C. gloeosporioides* infection. This further supports the notion that *MdRGA3* is crucial for apple resistance to *C. gloeosporioides*.

miRNAs, as key regulatory molecules, orchestrate a complex network of gene expression in response to pathogen infection, including in apples [39]. For example, *Md-miR156ab* and *Md-miR395* target *WRKY* transcription factors, thereby affecting resistance to *Alternaria alternata* by modulating the expression of pathogenesis-related (*PR*) genes [13]. Similarly, *Md-miR482* has been confirmed to regulate the expression of *NBS-LRR* genes, with overexpression of *miR482* attenuating disease resistance by inhibiting *MdTNL1* expression [12]. To our knowledge, there is no report about the involvement of *miR396* in the interaction between apple and pathogenic fungi. This study is the first to reveal the regulatory role of *MIR396d-p3* in apple–fungal interactions. In addition, *RGA3* (a member of the *R* gene family) and *UGT89A2* (a key regulator of secondary metabolism) were reported as *MIR396d-p3* target genes for the first time. This highlights the complexity of plant immune responses, which are mediated by both *R* genes and the regulation of secondary metabolite biosynthesis. This study not only fills the research gap regarding miRNA in apple—*C. gloeosporioides* interactions but also enriches the molecular basis of apple disease resistance mechanisms through integrating various regulatory networks.

In addition, several strategies can be employed to enhance disease resistance in plant breeding, including traditional breeding methods, marker-assisted selection, and various genetic engineering techniques. One particularly promising approach focuses on manipulating small RNA pathways. This involves either suppressing small RNAs that inhibit defense responses or boosting the expression of genes that confer resistance, thereby enhancing the plant's immune response and the ability to resist pathogenic bacteria.

5. Conclusions

In summary, this study reveals that *MIR396d-p3* negatively regulates apple resistance to *C. gloeosporioides* by suppressing the expression of *MdUGT89A2* and *MdRGA3*. Functional analyses demonstrated that overexpressing *MdUGT89A2* or *MdRGA3* enhances tolerance to *C. gloeosporioides*, while silencing *MdUGT89A2* or *MdRGA3* increases susceptibility to *C. gloeosporioides*. This study identifies a novel *MIR396d-p3-MdUGT89A2/MdRGA3* regulatory axis, deepening the understanding of the mechanism of miRNA in the interaction between apples and pathogenic fungi, and also provided references for potential resistance breeding sites.

Supplementary Materials: The following supporting information can be downloaded at: https://www.mdpi.com/article/10.3390/horticulturae11040351/s1, Supplemental material Figure S1: Statistics plants *miR396* sequences. Numeric distribution of *miR396s* across 52 plant species, with column height representing the quantity. Figure S2: Phylogenetic tree of plants *miR396* precursor sequences. Figure S3. Analysis of cis-acting elements in *MIR396d-p3* promoter. Figure S4: Phylogenetic tree of plants miR396 precursor sequences. Figure S5: Schematic diagrams of the expression constructs for *MdUGT89A2* and *MdRGA3* under the control of the 35S promoter and NOS—Ter terminator. Figure S6: Schematic illustrations of the RNAi constructs for *MdUGT89A2* and *MdRGA3*. Table S1: Description of the target transcripts of the *MIR396d-p3*. Table S2: Primers in this study.

Author Contributions: Writing—original draft preparation, B.Z.; methodology, B.Z. and J.T.; data curation and software, B.Z., J.T., Z.J. and Y.D.; writing—review and editing, B.Z., J.T. and J.C.; software—B.Z., Y.D., J.C.; supervision: Z.Z.; conceptualization, B.Z. and Z.Z.; resources and investigation, Z.Z. All authors have read and agreed to the published version of the manuscript.

Funding: This work was supported by Agricultural Science and Technology Innovation Program (CAAS-ASTIP-2016-RIP) and the Asian regional cooperation special projects.

Data Availability Statement: Data is contained within the article and Supplementary Materials.

Conflicts of Interest: The authors declare no conflicts of interest.

References

1. Hamada, N.A.; Moreira, R.R.; Nesi, C.N.; May De Mio, L.L. Pathogen Dispersal and Glomerella Leaf Spot Progress Within Apple Canopy in Brazil. *Plant Dis.* **2019**, *103*, 3209–3217. [CrossRef] [PubMed]
2. Shi, J.; Zhang, F.; Su, Y.; Jiang, Q.; Yuan, Y.; Nie, X.; Zhou, Y.; Zhang, X.; Wang, Z.; Wang, F.; et al. MdIPT8, an Isopentenyl Transferase Enzyme, Enhances the Resistance of Apple to Colletotrichum Gloeosporioides Infection. *Sci. Hortic.* **2022**, *303*, 111245. [CrossRef]
3. Shang, S.; Liu, G.; Zhang, S.; Liang, X.; Zhang, R.; Sun, G. A Fungal CFEM-containing Effector Targets NPR1 Regulator NIMIN2 to Suppress Plant Immunity. *Plant Biotechnol. J.* **2023**, *22*, 82–97. [CrossRef]
4. Wang, B.; Li, B.-H.; Dong, X.-L.; Wang, C.-X.; Zhang, Z.-F. Effects of Temperature, Wetness Duration, and Moisture on the Conidial Germination, Infection, and Disease Incubation Period of Glomerella Cingulata. *Plant Dis.* **2015**, *99*, 249–256. [CrossRef] [PubMed]
5. Song, X.; Li, Y.; Cao, X.; Qi, Y. MicroRNAs and Their Regulatory Roles in Plant–Environment Interactions. *Annu. Rev. Plant Biol.* **2019**, *70*, 489–525. [CrossRef]
6. Qiao, Y.; Xia, R.; Zhai, J.; Hou, Y.; Feng, L.; Zhai, Y.; Ma, W. Small RNAs in Plant Immunity and Virulence of Filamentous Pathogens. *Annu. Rev. Phytopathol.* **2021**, *59*, 265–288. [CrossRef]

7. Yu, X.; Hou, Y.; Chen, W.; Wang, S.; Wang, P.; Qu, S. Malus Hupehensis miR168 Targets to ARGONAUTE1 and Contributes to the Resistance against Botryosphaeria Dothidea Infection by Altering Defense Responses. *Plant Cell Physiol.* **2017**, *58*, 1541–1557. [CrossRef]
8. Yu, X.; Gong, H.; Cao, L.; Hou, Y.; Qu, S. MicroRNA397b Negatively Regulates Resistance of Malus Hupehensis to Botryosphaeria Dothidea by Modulating MhLAC7 Involved in Lignin Biosynthesis. *Plant Sci.* **2020**, *292*, 110390. [CrossRef]
9. Zhou, T.; Cao, L.; Hu, K.; Yu, X.; Qu, S. miR164–NAC21/22 Module Regulates the Resistance of Malus Hupehensis against Alternaria Alternata by Controlling Jasmonic Acid Signaling. *Plant Sci.* **2023**, *330*, 111635. [CrossRef]
10. Yu, X.; Hou, Y.; Cao, L.; Zhou, T.; Wang, S.; Hu, K.; Chen, J.; Qu, S. MicroRNA Candidate miRcand137 in Apple Is Induced by *Botryosphaeria dothidea* for Impairing Host Defense. *Plant Physiol.* **2022**, *189*, 1814–1832. [CrossRef]
11. Zhang, Q.; Ma, C.; Zhang, Y.; Gu, Z.; Li, W.; Duan, X.; Wang, S.; Hao, L.; Wang, Y.; Wang, S.; et al. A Single-Nucleotide Polymorphism in the Promoter of a Hairpin RNA Contributes to *Alternaria alternata* Leaf Spot Resistance in Apple (*Malus* × *Domestica*). *Plant Cell* **2018**, *30*, 1924–1942. [CrossRef] [PubMed]
12. Liu, F.; Tang, J.; Li, T.; Zhang, Q. The microRNA miR482 Regulates NBS-LRR Genes in Response to ALT1 Infection in Apple. *Plant Sci.* **2024**, *343*, 112078. [CrossRef] [PubMed]
13. Zhang, Q.; Li, Y.; Zhang, Y.; Wu, C.; Wang, S.; Hao, L.; Wang, S.; Li, T. Md-miR156ab and Md-miR395 Target WRKY Transcription Factors to Influence Apple Resistance to Leaf Spot Disease. *Front. Plant Sci.* **2017**, *8*, 526. [CrossRef] [PubMed]
14. Zhang, Y.; Zhang, Q.; Hao, L.; Wang, S.; Wang, S.; Zhang, W.; Xu, C.; Yu, Y.; Li, T. A Novel miRNA Negatively Regulates Resistance to Glomerella Leaf Spot by Suppressing Expression of an NBS Gene in Apple. *Hortic. Res.* **2019**, *6*, 93. [CrossRef]
15. Soto-Suárez, M.; Baldrich, P.; Weigel, D.; Rubio-Somoza, I.; San Segundo, B. The Arabidopsis miR396 Mediates Pathogen-Associated Molecular Pattern-Triggered Immune Responses against Fungal Pathogens. *Sci. Rep.* **2017**, *7*, 44898. [CrossRef]
16. Dai, Z.; Tan, J.; Zhou, C.; Yang, X.; Yang, F.; Zhang, S.; Sun, S.; Miao, X.; Shi, Z. The OsmiR396–OsGRF8–OsF3H-flavonoid Pathway Mediates Resistance to the Brown Planthopper in Rice (*Oryza sativa*). *Plant Biotechnol. J.* **2019**, *17*, 1657–1669. [CrossRef]
17. Zhang, Y.; Xiao, T.; Yi, F.; Yu, J. SimiR396d Targets SiGRF1 to Regulate Drought Tolerance and Root Growth in Foxtail Millet. *Plant Sci.* **2023**, *326*, 111492. [CrossRef]
18. Noon, J.B.; Hewezi, T.; Baum, T.J. Homeostasis in the Soybean miRNA396–*GRF*Network Is Essential for Productive Soybean Cyst Nematode Infections. *J. Exp. Bot.* **2019**, *70*, 1653–1668. [CrossRef]
19. Dimunová, D.; Matoušková, P.; Podlipná, R.; Boušová, I.; Skálová, L. The Role of UDP-Glycosyltransferases in Xenobioticresistance. *Drug Metab. Rev.* **2022**, *54*, 282–298. [CrossRef]
20. Bowles, D.; Isayenkova, J.; Lim, E.-K.; Poppenberger, B. Glycosyltransferases: Managers of Small Molecules. *Curr. Opin. Plant Biol.* **2005**, *8*, 254–263. [CrossRef]
21. Huang, X.; Wang, Y.; Lin, J.; Chen, L.; Li, Y.; Liu, Q.; Wang, G.; Xu, F.; Liu, L.; Hou, B. The Novel Pathogen-responsive Glycosyltransferase UGT73C7 Mediates the Redirection of Phenylpropanoid Metabolism and Promotes *SNC1*-dependent Arabidopsis Immunity. *Plant J.* **2021**, *107*, 149–165. [CrossRef] [PubMed]
22. Bethke, G.; Huang, Y.; Hensel, G.; Heinen, S.; Liu, C.; Wyant, S.R.; Li, X.; Quin, M.B.; McCormick, S.; Morrell, P.L.; et al. UDP-Glucosyltransferase HvUGT13248 Confers Type II Resistance to *Fusarium Graminearum* in Barley. *Plant Physiol.* **2023**, *193*, 2691–2710. [CrossRef] [PubMed]
23. Jiang, H.; Qu, S.; Liu, F.; Sun, H.; Li, H.; Teng, W.; Zhan, Y.; Li, Y.; Han, Y.; Zhao, X. Multi-omics Analysis Identified the *GmUGT88A1* Gene, Which Coordinately Regulates Soybean Resistance to Cyst Nematode and Isoflavone Content. *Plant Biotechnol. J.* **2025**. *early view*. [CrossRef]
24. McHale, L.; Tan, X.; Koehl, P.; Michelmore, R.W. Plant NBS-LRR Proteins: Adaptable Guards. *Genome Biol.* **2006**, *7*, 212. [CrossRef]
25. Huang, S.; Jia, A.; Ma, S.; Sun, Y.; Chang, X.; Han, Z.; Chai, J. NLR Signaling in Plants: From Resistosomes to Second Messengers. *Trends Biochem. Sci.* **2023**, *48*, 776–787. [CrossRef]
26. Wu, J.; Ji, Z.; Wang, N.; Chi, F.; Xu, C.; Zhou, Z.; Zhang, J. Identification of Conidiogenesis-Associated Genes in Colletotrichum Gloeosporioides by Agrobacterium Tumefaciens-Mediated Transformation. *Curr. Microbiol.* **2016**, *73*, 802–810. [CrossRef]
27. Zhang, B.; Zhang, M.; Jia, X.; Hu, G.; Ren, F.; Fan, X.; Dong, Y. Integrated Transcriptome and Metabolome Dissecting Interaction between Vitis Vinifera L. and Grapevine Fabavirus. *Int. J. Mol. Sci.* **2023**, *24*, 3247. [CrossRef]
28. Daccord, N.; Celton, J.-M.; Linsmith, G.; Becker, C.; Choisne, N.; Schijlen, E.; van de Geest, H.; Bianco, L.; Micheletti, D.; Velasco, R.; et al. High-Quality de Novo Assembly of the Apple Genome and Methylome Dynamics of Early Fruit Development. *Nat. Genet.* **2017**, *49*, 1099–1106. [CrossRef]
29. Li, W.; Jia, Y.; Liu, F.; Wang, F.; Fan, F.; Wang, J.; Zhu, J.; Xu, Y.; Zhong, W.; Yang, J. Integration Analysis of Small RNA and Degradome Sequencing Reveals MicroRNAs Responsive to Dickeya Zeae in Resistant Rice. *Int. J. Mol. Sci.* **2019**, *20*, 222. [CrossRef]
30. Dai, X.; Zhao, P.X. psRNATarget: A Plant Small RNA Target Analysis Server. *Nucleic Acids Res.* **2011**, *39*, W155–W159. [CrossRef]
31. Chen, C.; Wu, Y.; Li, J.; Wang, X.; Zeng, Z.; Xu, J.; Liu, Y.; Feng, J.; Chen, H.; He, Y.; et al. TBtools-II: A "One for All, All for One" Bioinformatics Platform for Biological Big-Data Mining. *Mol. Plant* **2023**, *16*, 1733–1742. [CrossRef] [PubMed]

32. Jefferson, R.A.; Kavanagh, T.A.; Bevan, M.W. GUS Fusions: Beta-Glucuronidase as a Sensitive and Versatile Gene Fusion Marker in Higher Plants. *EMBO J.* **1987**, *6*, 3901–3907. [CrossRef] [PubMed]
33. Reid, K.E.; Olsson, N.; Schlosser, J.; Peng, F.; Lund, S.T. An Optimized Grapevine RNA Isolation Procedure and Statistical Determination of Reference Genes for Real-Time RT-PCR during Berry Development. *BMC Plant Biol.* **2006**, *6*, 27. [CrossRef]
34. Liu, Y.; Yan, J.; Wang, K.; Li, D.; Yang, R.; Luo, H.; Zhang, W. MiR396-*GRF* Module Associates with Switchgrass Biomass Yield and Feedstock Quality. *Plant Biotechnol. J.* **2021**, *19*, 1523–1536. [CrossRef]
35. Wang, L.; Hou, J.; Xu, H.; Zhang, Y.; Huang, R.; Wang, D.; He, X.-Q. The PtoTCP20-miR396d-PtoGRF15 Module Regulates Secondary Vascular Development in Populus. *Plant Commun.* **2023**, *4*, 100494. [CrossRef]
36. Sun, L.; Zhu, M.; Zhou, X.; Gu, R.; Hou, Y.; Li, T.; Huang, H.; Yang, R.; Wang, S.; Zhao, W. The miR396a–SlGRF8 Module Regulates Sugar Accumulation in the Roots via SlSTP10 during the Interaction between Root-knot Nematodes and Tomato Plants. *J. Integr. Plant Biol.* **2024**, *66*, 2701–2715. [CrossRef]
37. Wang, J.; Song, W.; Chai, J. Structure, Biochemical Function, and Signaling Mechanism of Plant NLRs. *Mol. Plant* **2023**, *16*, 75–95. [CrossRef]
38. Zhang, J.; Coaker, G.; Zhou, J.-M.; Dong, X. Plant Immune Mechanisms: From Reductionistic to Holistic Points of View. *Mol. Plant* **2020**, *13*, 1358–1378. [CrossRef]
39. Padmanabhan, C.; Zhang, X.; Jin, H. Host Small RNAs Are Big Contributors to Plant Innate Immunity. *Curr. Opin. Plant Biol.* **2009**, *12*, 465–472. [CrossRef]

Disclaimer/Publisher's Note: The statements, opinions and data contained in all publications are solely those of the individual author(s) and contributor(s) and not of MDPI and/or the editor(s). MDPI and/or the editor(s) disclaim responsibility for any injury to people or property resulting from any ideas, methods, instructions or products referred to in the content.